Influence of hydrostatic pressure on hidden order, the Kondo lattice, and magnetism in $URu_2Si_{2-x}P_x$

Greta L. Chappell,[1,2] A. Gallagher,[1,2] D. E. Graf,[1] Peter Riseborough,[3] and Ryan E. Baumbach[1,2,*]

[1]*National High Magnetic Field Laboratory, Florida State University, Tallahassee, Florida 32310, USA*

[2]*Department of Physics, Florida State University, Tallahassee, Florida 32306, USA*

[3]*Department of Physics, Temple University, Philadelphia, Pennsylvania 19122, USA*

(Received 17 September 2020; accepted 14 December 2020; published 31 December 2020)

Within the chemical substitution series $URu_2Si_{2-x}P_x$, there is an evolution in the ground-state behavior from hidden ordered (HO) for $x \lesssim 0.03$, to Kondo lattice behavior with no ordering (NO) for $0.03 \lesssim x \lesssim 0.26$, to antiferromagnetism (AFM-2) for $0.26 \lesssim x \lesssim 0.5$ [A. Gallagher *et al.*, Nat. Commun. **7**, 10712 (2016); A. Gallagher *et al.*, J. Phys.: Condens. Matter **29**, 024004 (2016)]. To better understand what factors control this behavior, temperature-dependent electrical resistivity measurements are performed for this series under applied pressures P up to 20.5 kbar. Specimens in the HO x region show similarities to the parent compound, where HO transforms into antiferromagnetism (AFM-1) at a critical pressure (P_c). P_c decreases with increasing x and collapses towards $P = 0$ near $x \approx 0.03$, suggesting that AFM-1 occurs at ambient pressure for this concentration. No pressure-induced phase transitions are observed in the NO x region and the AFM-2 state is only weakly suppressed by P. Measurements further reveal that AFM-1 and AFM-2 are distinct from each other. Calculations of the wave functions using the tight-binding Hartree-Fock approximation are performed and show (i) that the radial probability distributions for the phosphorus ions are more tightly bound than those for the silicon and (ii) that the energy difference between the orbitals decreases with increasing x. The cumulative effect of these two factors is that Si $\rightarrow$ P substitution decreases the hybridization strength, which correlates with the weakening of HO. At large x, additional effects such as electrical charge tuning also play an important role in determining the ground-state behavior.

DOI: 10.1103/PhysRevB.102.245152

I. INTRODUCTION

URu_2Si_2 is well known for its transition into the hidden order (HO) state near $T_0 \approx 17.4$ K and the superconductivity that occurs below $T_c = 1.5$ K [1–3]. Thermodynamic and electrical transport measurements show that HO emerges through a bulk second-order phase transition [1,4], yet many measurements show that it does not involve a magnetic order parameter (e.g., neutron scattering [5] and nuclear magnetic resonance [6]). Experiments, such as angle-resolved photoemission spectroscopy [7–10], infrared spectroscopy [11], scanning tunneling microscopy [12,13], and optical conductivity [11,14,15], reveal the importance of the hybridization between the uranium f electrons and the conduction electrons. Recent electronic Raman spectroscopy measurements have further advanced the field by showing that HO is a type of commensurate chirality density wave state that breaks local vertical and diagonal reflection symmetries at the uranium sites [16]. However, even after substantial efforts, which have spanned over three decades, the HO state and its relationship to more common ordered states such as magnetism remain enigmatic [17,18].

Numerous experiments that probe HO using an applied magnetic field, applied pressure, and chemical substitution have highlighted its uniqueness and its close proximity to magnetic ordering in the electronic phase space. For instance, an applied magnetic field H suppresses HO and produces a cascade of complex magnetically ordered states above $H = 35$ T [19–22], while applied pressure transforms HO into antiferromagnetism (AFM-1) around 10 kbar [23–26]. Isoelectronic chemical substitution at the Ru site with Fe or Os produces a similar phase diagram, and based on this it has been inferred that strengthening hybridization is responsible for the conversion from HO to AFM-1 [27–31]. In contrast, nonisoelectronic substitutions at the Ru site using Rh [32–37] or Ir [33] (i.e., electron doping) suppresses T_0, stabilizes AFM-1, produces a Kondo lattice without an ordered ground state, and eventually stabilizes another antiferromagnetic region (AFM-2). Substitutions with Tc or Re [33,38–43] (i.e., hole doping) suppress T_0 and stabilize ferromagnetism. Finally, chemical substitution at the uranium site with rare earth elements shows the importance of the uranium $5f$ orbitals to the stability of HO [44–46].

These earlier works provide insights but are complicated in each case because the f- and d-electron states are directly disrupted. To avoid this complexity, the chemical substitution series $URu_2Si_{2-x}P_x$ was recently investigated [47,48]. There it was proposed that the primary tuning parameter is a combination of electron doping at the s/p sites and lattice compression. Experiments show that for low phosphorus concentrations ($x \leqslant 0.03$), HO is slightly suppressed and abruptly collapses towards zero temperature near $x = 0.03$ (see Fig. 1, inset); further substitution ($0.03 \lesssim x \lesssim 0.26$) results in Kondo

*baumbach@magnet.fsu.edu

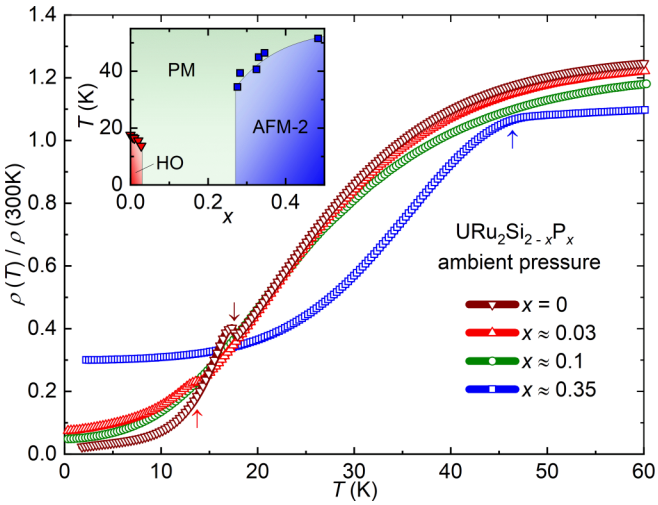

FIG. 1. The room-temperature-normalized electrical resistivity $\rho(T)/\rho(300\ \mathrm{K})$ for $URu_2Si_{2-x}P_x$ at ambient pressure for select concentrations in the hidden order, no order, and antiferromagnetic x regions ($x = 0$, 0.03, 0.1, and 0.35). Arrows indicate the transition temperature T_0 for $x = 0$ and 0.03 and T_{N2} for $x \approx 0.35$. Inset: Transition temperature and chemical concentration T-x phase diagram from Ref. [48].

lattice behavior with no ordered (NO) ground state, and for $x \gtrsim 0.26$ AFM-2 emerges at temperatures $T_{N2} \gtrsim 40$ K. Together with earlier results from Ru → Rh, Ir substitution studies [32,33,35–37] this suggests that electron doping results in a quasiuniversal electronic phase diagram.

In the current study, we present results addressing the influence of applied pressure ($P \leqslant 20.5$ kbar) in $URu_2Si_{2-x}P_x$. For concentrations that exhibit HO, applied pressure produces phenomena that are similar to those of the parent compound: HO is converted to antiferromagnetism (AFM-1), where the critical pressure for this transformation decreases towards zero pressure with increasing phosphorus content. Within the NO x region, applied pressure does not induce any ordered states and slightly perturbs the underlying Kondo lattice up to $P = 13.5$ kbar. Within the large-x region, AFM-2 is slightly suppressed with P and exhibits behavior that is distinct from that of AFM-1. In order to better understand these results, tight-binding Hartree-Fock calculations were performed to assess the hybridization between the U, Si, and P orbitals. While these calculations do not account for potential changes in the electronic structure due to charge doping, they show that the Si → P substitution causes a decrease in the hybridization strength. This is consistent with our observation in the HO x region that T_0 decreases with increasing x, in contrast to what is seen under applied pressure and for isoelectronic chemical substitution at the Ru site where the hybridization strength (and T_0) increases. Thus, these results provide new insights into the quasiuniversal phase diagram that results from Si → P and Ru → Co/Ir substitution and may also point the way towards stabilizing HO in related compounds that exhibit AFM in their natural form.

II. EXPERIMENTAL METHODS

Single crystals of $URu_2Si_{2-x}P_x$ were grown using a molten indium flux in a resistive tube furnace as reported previously [47,48]. The actual chemical composition was determined using energy dispersive x-ray spectroscopy with scanning electron microscopy measurements. Electrical resistivity $\rho(T)$ measurements were performed on single-crystal specimens for concentrations $x = 0$ and $x \approx 0.01$, 0.02, 0.03, 0.1, 0.2, 0.33, and 0.35 using a standard four-wire configuration with the current applied along the crystalline *ab* plane in a Quantum Design Physical Property Measurement System at temperatures $T = 1.8$–300 K. Applied pressures up to 20.5 kbar were achieved using a double-wall beryllium copper clamped piston cylinder cell and a quasihydrostatic pressure environment was provided with Daphne 7575 oil, which has a solidification pressure of 40.5 kbar at room temperature and is otherwise similar in physical properties to Daphne 7474 oil [49]. The pressure was determined using fluorescence from a ruby crystal that was located between the $URu_2Si_{2-x}P_x$ samples. The pressure dependence of the R_1 fluorescence line is well established [50] and the shift in wavelength of the R_1 line from ambient pressure was measured using a 523-nm green laser.

III. RESULTS

Each region of the $URu_2Si_{2-x}P_x$ temperature vs phosphorus concentration T-x phase space at ambient pressure has a distinct signature in the electrical resistivity $\rho(T)$ at low T, as shown in Fig. 1. For the well-established case of $x = 0$, $\rho(T)$ features a broad maximum due to Kondo-lattice behavior with $T_{coh} \approx 70$ K and a sharp peak indicating the occurrence of the HO phase with $T_0 = 17.4$ K [T_0 is defined as the minimum in $\partial\rho/\partial T$; see Fig. 2(b)]. As x increases, the Kondo lattice behavior is preserved for all x, while the HO peak decreases in amplitude and gradually shifts to lower temperatures. In the NO x region, $\rho(T)$ is smooth and quadratic at low T, and in the AFM-2 x region it exhibits a kneelike bend due to a reduction of magnetic scattering of conduction electrons at the antiferromagnetic ordering temperature T_{N2} [T_{N2} is defined as the sharp increase in $\partial\rho/\partial T$; see Fig. 2(q)]. Here, we expand the T-x phase diagram along the pressure P axis through $\rho(T)$ measurements at fixed P for $x = 0$, 0.01, 0.02, 0.03, 0.1, 0.2, 0.33, and 0.35 (Fig. 2). The T-x-P phase diagram shows that the HO phase transforms into antiferromagnetism (AFM-1), similarly to the parent compound under applied pressure, the NO behavior is robust and no additional ordering appears in this x region to connect AFM-1 and AFM-2, and the antiferromagnetism at large x (AFM-2) is gradually suppressed with P.

The behavior of URu_2Si_2 ($x = 0$) under applied pressure is well established: the transition temperature increases with P at a constant rate of ∼0.10 K/kbar and there is an increase in the rate to ∼0.25 K/kbar at the critical pressure $P_c = 10$–15 kbar, where HO transforms to AFM-1 [23,25,51,52]. Our data show similar behavior [Figs. 2(a) and 2(b)], and we additionally observe that the peak feature in $\rho(T)$ progressively changes shape up to 11.8 kbar, where $\partial\rho/\partial T$ abruptly broadens [Fig. 2(b)]. To quantify this change, we show the

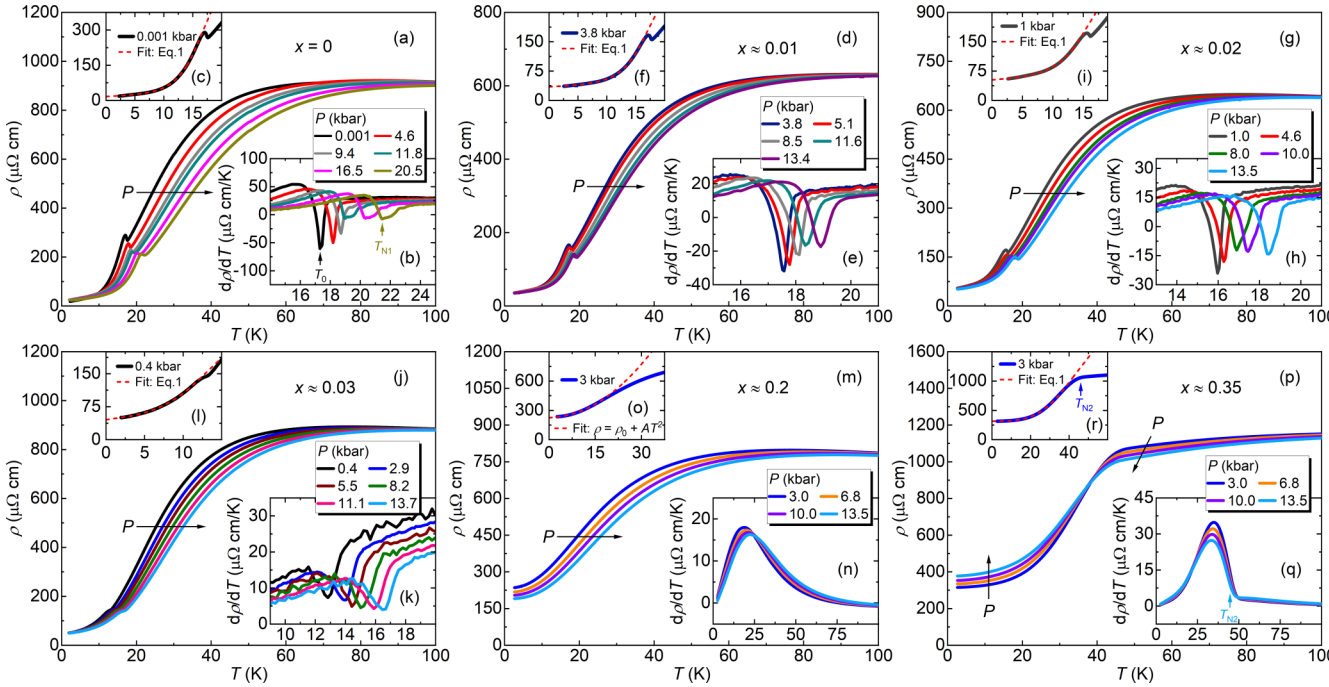

FIG. 2. The temperature-dependent electrical resistivity $\rho(T)$ at various pressures P for $URu_2Si_{2-x}P_x$: (a) $x = 0$, (d) $x \approx 0.01$, (g) $x \approx 0.02$, (j) $x \approx 0.03$, (m) $x \approx 0.2$, and (p) $x \approx 0.35$. The samples $x \approx 0.1$ and 0.33 for the NO and AFM-2 regions, respectively, were measured and their results are similar to those for $x \approx 0.2$ and 0.35, therefore they are not shown. Black arrows indicate the direction of applied pressure. Insets: The derivative of the data with respect to temperature $\partial\rho/\partial T$ zoomed in on the HO transition (b, e, h, k), the low-T region of no ordering (n), and the AFM-2 transition (q). For clarity, several measured pressure curves have been omitted.

pressure dependence of the peak height $\Delta\rho/\rho_{\min}$ and width W in Fig. 3(c) and its inset, where the height is the difference between the local maximum $\rho_{\max}$ and the local minimum $\rho_{\min}$ and scaled by $\rho_{\min}$. The peak height decreases in the HO phase, nearly flattens at 11.8 kbar, and subtly increases in the AFM-1 phase. In addition, there is an abrupt increase in W between 9.4 and 11.8 kbar. Based on these features, and combined with the change in slope of the ordering temperature, we define $P_c = 10.6$ kbar with the width of possible values indicated by the bars in Figs. 3(c) and 4.

Results for the other HO x-region samples are shown in Figs. 2(d), 2(g) and 2(j). First, we note that $T_{coh}(P)$ linearly increases for all x values in the HO region, suggesting that the hybridization strength between the f and the conduction electrons increases with increasing P. At lower temperatures, the pressure-dependent results for $x \approx 0.01$ and 0.02 are similar to those for $x = 0$: the transition temperature increases with P and there is a kink in their T-P lines at $P_c = 9.35$ and 5.7 kbar, respectively. Although the differences in the behavior of $\partial\rho/\partial T$ between the HO and the high-pressure region is less obvious than for $x = 0$, close inspection of the data [Figs. 3(a) and 3(b)] reveals trends that are similar to what is seen for $x = 0$ for $\Delta\rho/\rho_{\min}$ and W [Fig. 3(c)]. This suggests that, similarly to $x = 0$, applied pressure converts HO into AFM-1, and we define P_c and its width in the same way as described for $x = 0$. From this, it is seen that the temperature and pressure energy scales for the hidden order phase are directly linked together, as seen in the tendency of both to be suppressed with increasing x.

We unexpectedly find a different result for $x \approx 0.03$ [Figs. 2(j) and 2(k)], where the $\partial\rho/\partial T$ curves are broad in comparison to those seen at lower x, and there is no evidence for a transition from HO to AFM-1 in the T-P phase boundary line. The reason for this is not obvious; however, even for $P = 0$ their shape is similar to what is seen in the AFM-1 state at lower x, suggesting that this concentration may already exhibit AFM order even at ambient pressure. This would be similar to what is observed in the Ru → Rh series at ambient pressure for concentrations near the collapse of the HO phase [36,37], although in our series the associated x range is smaller. It is also possible to extrapolate from the values of $P_c(x)$ that the hidden order to AFM-1 transition might collapse to zero pressure by $x = 0.03$ (Fig. 4).

Similarly to earlier studies, we fit $\rho(T)$ (covering ~90% T_0) using the expression

$$\rho(T) = \rho_0 + AT^2 + B\frac{T}{\Delta}\left(1 + \frac{T}{\Delta}\right)e^{-\Delta/T}, \qquad (1)$$

which includes the residual resistivity ρ_0, a Fermi liquid term AT^2, and an exponential term with an energy gap Δ [4,23,25,51,52] [dashed red lines in Figs. 2(c), 2(f) 2(i), 2(l)]. Although it has been established that HO is nonmagnetic [17,18], Δ is thought to represent the gap for bosonic excitations of the order parameter. For all three concentrations in the HO x region, a similar fit to the data was performed using Eq. (1) and the resulting $\Delta(P)$ behavior is summarized with the $x = 0$ data (Fig. 4, inset). We first point out that, in general, their behavior is similar to that at $x = 0$, where Δ increases with the pressure during the transformation from HO to AFM-1, and the pressure where the increase occurs precedes P_c (marked by the black arrow at the top axis). This provides further evidence that the behavior at $x \approx 0.01$ and

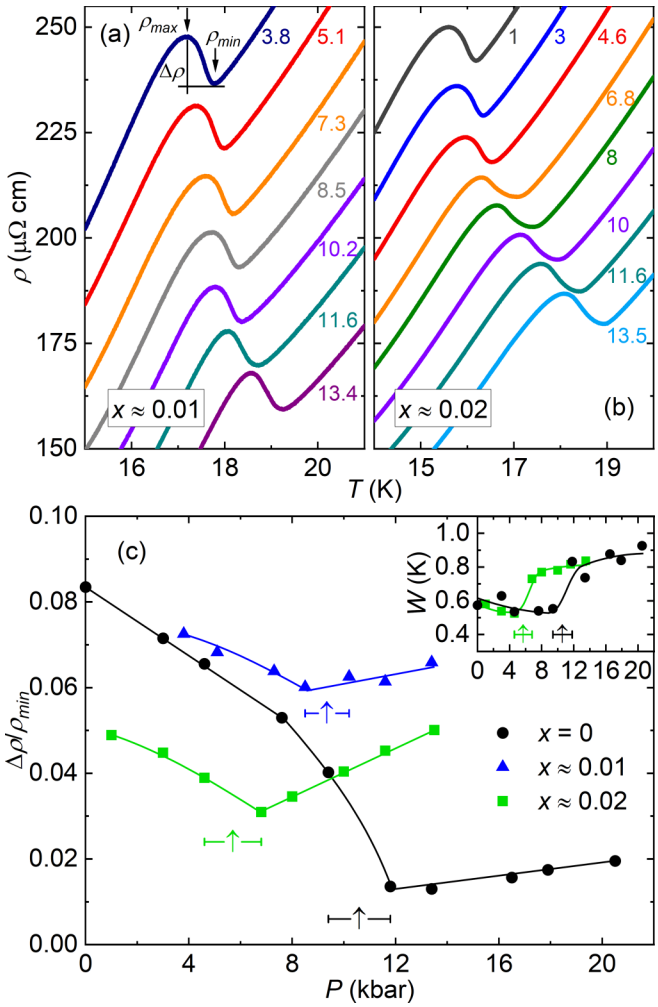

FIG. 3. (a,b) A zoom-in on the electrical resistivity ρ vs temperature T for $URu_2Si_{2-x}P_x$ in the vicinity of the ordering temperature for $x \approx 0.01$ and 0.02, respectively. (c) The pressure dependence of the peak height $\Delta\rho/\rho_{min}$ as defined in (a) for $x = 0$, 0.01, and 0.02. Inset: Temperature width W at the phase transition. Results for $x \approx 0.01$ are similar to those for $x = 0$ but are omitted for clarity. Lines are guides for the eye, arrows indicate the critical pressure P_c for the HO $\rightarrow$ AFM-1 transition, and spanning bars represent the range of pressure where P_c could be defined based on the method described in the text.

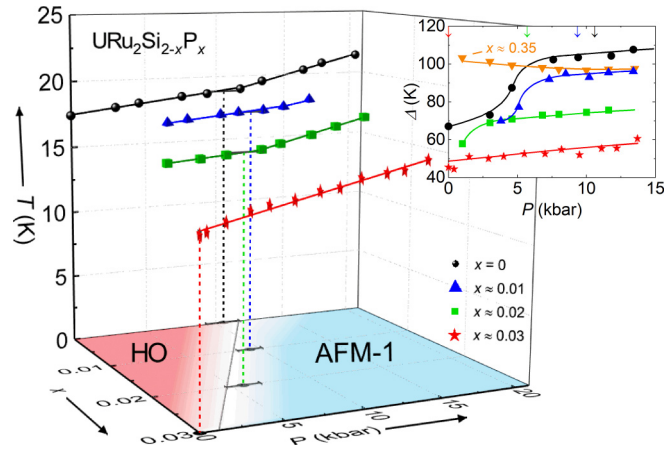

FIG. 4. Transition temperature $T_{0,N1}$ vs phosphorus concentration x vs applied pressure P phase diagram for $URu_2Si_{2-x}P_x$ for $x = 0$, 0.01, 0.02, and 0.03 with linear fits (solid lines). The critical pressure P_c for the HO $\rightarrow$ AFM-1 transition is indicated by the dashed vertical lines and gray circles with spanning bars [the same as in Fig. 3(c)], and the solid gray line is a linear fit to P_c that marks the HO/AFM-1 phase boundary. Inset: The energy gap parameter Δ, extracted from fits to data with Eq. (1) as described in the text, for these concentrations and for $x \approx 0.35$. The error bars, determined from the fitting algorithm, are smaller than the symbols, except for $x \approx 0.03$.

0.02 is analogous to that of the parent compound. It is also shown that the pressure where Δ increases is suppressed with increasing x and that the absolute value of Δ decreases. This emphasizes that both the characteristic energy scales, T_0 and P_c, are suppressed by phosphorus substitution. Finally, fits for the $x \approx 0.03$ curves show that Δ is further suppressed and that there is no rapid increase that would indicate a transformation from HO to AFM-1. This reinforces the view that this concentration is already in the AFM-1 state at ambient pressure.

Results for samples in the NO region are displayed in Fig. 2(m). Here, applied pressure has the effect of suppressing the absolute value of $\rho(T)$ down to the lowest temperatures while shifting T_{coh} to higher temperatures. Fits to $\rho(T)$ up to 40 K were carried out using a simple Fermi-liquid function, $\rho(T) = \rho_0 + AT^2$ [see Fig. 2(o)], and yielded $\rho_0 = 228.5\ \mu\Omega$ cm and $A = 0.606\ \mu\Omega\,\text{cm/K}^2$ at $P = 3$ kbar, which change at a rate of $-2.85\ \mu\Omega$ cm/kbar and $-0.013\ \mu\Omega\,\text{cm/K}^2$ kbar, respectively. Importantly, there is no evidence for the emergence of an ordered ground state up to 14 kbar. The finding that the Kondo lattice behavior is robust against pressure and no ordered states appear shows that (i) while the Kondo lattice provides the environment for HO, it is not the only criterion for this phase to appear, and (ii) the pressure-induced AFM-1 in the HO x samples is not obviously connected to the AFM-2 phase observed at large x and at ambient pressure. Measurements to even higher pressures would be of interest to determine how far this trend persists or if other ordered states appear.

Results for samples in the AFM-2 region are displayed in Fig. 2(p). Here, applied pressure slowly suppresses T_{N2} and $T_{coh}(P)$ remains roughly constant, while the residual resistivity slowly increases. Importantly, both the shape of this transition and its evolution with P are distinct from what is seen for the pressure-induced AFM-1 in the HO x samples. This indicates that these ordered states are different from those seen at low x and likely not directly connected to them in the T-x-P phase space. Indeed, the magnetism that is observed for the structurally related compounds URh_2Si_2 [53], UIr_2Si_2 [53,54], and UCo_2Si_2 [55] results in electrical transport behavior that is similar to that seen in the AFM x region, suggesting a connection between these types of behaviors. Fits to the data were also carried out using Eq. (1) to 80% of T_{N2} in order to extract Δ, and the result is shown in the inset in Fig. 4 (downward orange triangles). The ambient pressure Δ is significantly larger than those seen at lower x and follows the opposite trend of decreasing with increasing P, further

demonstrating that this magnetic order is distinct from the pressure-induced AFM-1 seen in the HO x samples.

IV. DISCUSSION

The full T-x-P phase diagram constructed from the above measurements consists of (i) the low-x HO/AFM-1 region that collapses with both increasing x and increasing P (Fig. 4), (ii) a robust Kondo lattice region with no ordered ground state, and (iii) a second distinct AFM-2 region that strengthens with increasing x but is gradually suppressed with P. First, we focus on the HO/AFM-1 region. As shown previously, the phase boundaries between the paramagnetic and the ordered states have linear slopes, and fits to the data (solid lines in Fig. 4) below and above P_c yield slopes of ~ 0.11 K/kbar in the HO x region and ~ 0.26 K/kbar in the AFM x region. These slopes are persistent for $x \lesssim 0.03$ and also consistent with results from other chemical substitutions series where HO/AFM-1 phases were observed [27,56]. P_c is suppressed with increasing x and is extrapolated to collapse towards zero pressure near $x \approx 0.03$. This is consistent with there being no change in the shape of $\rho(T)$ around the ordering temperature and with the phase boundary exhibiting a single slope for all P that is consistent with the AFM-1 phase. Thus these measurements show that Si $\rightarrow$ P substitution not only weakens HO at zero pressure, but also suppresses the energy scale to convert HO to AFM-1.

Some insight into this evolution is gained by contrasting it with what is seen for Ru $\rightarrow$ Fe chemical substitution under applied pressure, where both tuning parameters initially enhance T_0 and eventually drive a conversion into the AFM-1 state. This is believed to show that (i) the chemical pressure P_{ch} is equivalent to the applied pressure, (ii) the parameters are additive such that $P_{ch}(x_c) + P_c(x) = P_c(x = 0)$, and (iii) these both increase the hybridization strength between the f and the conduction electrons [56]. Ru $\rightarrow$ Os chemical substitution also produces a similar T-x phase diagram [28], and this has been understood as resulting from an enhancement of the hybridization strength due to the more spatially extended osmium $5d$ orbitals and the possible impact of a strengthened spin-orbit coupling [30]. Based on these combined results, it would be natural to infer that the decreasing unit cell volume that is seen in the Si $\rightarrow$ P substitution series would lead to an enhanced hybridization strength and a similar T-x-P phase diagram. However, this is in contrast to what is observed experimentally and suggests that other factors influence the behavior of this system.

In order to better understand the impact of Si $\rightarrow$ P substitution on the hybridization between the U $5f$ electrons and the conduction electrons, tight-binding Hartree-Fock calculations were performed [57–62]. The radial probability distributions for the uranium, silicon, and phosphorus orbitals are displayed in Fig. 5, where it is shown that the phosphorus radial probability is more tightly bound than that of the silicon orbital. This results in a decreased overlap with the uranium radial function and thus a decrease in the hybridization strength. However, calculations also show that the energy difference also decreases (Table I), which increases the hybridization strength by 20%. Calculating the two-center tight-binding integrals with the U $5f$ and Si or P $3p$ Hartree-Fock wave functions, we find that the cumulative effect of these factors with the bond orientations [63–67] is that the hybridization energies decrease due to P substitution. This can be correlated with the suppression of T_0 with increasing x and is consistent with the view that T_0 is enhanced with increasing hybridization strength and suppressed with decreasing hybridization strength.

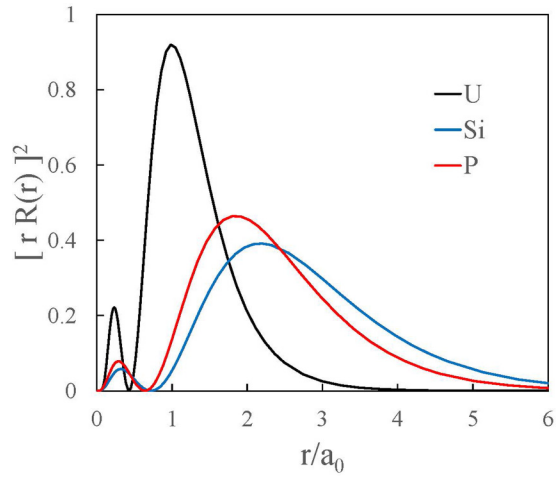

FIG. 5. The radial probability distributions for U, Si, and P expressed in atomic units.

Upon moving to the larger-x region of the phase diagram, it is likely that additional effects such as electrical charge tuning also play an important role. In the simplest model, the underlying band structure of the parent URu_2Si_2 would be preserved across the entire T-x phase diagram, the replacement of Si with P would raise the Fermi energy, and eventually a Fermi surface reconstruction would occur as different branches of the band structure are traversed. This alone might account for the appearance of both the NO and the AFM-2 x regions if the different low-temperature states result from varying Fermi surface nesting wave vectors. However, our results suggest that a more realistic model also includes a decreasing hybridization strength, which further complicates this evolution. Even without a detailed understanding of how this occurs, it nonetheless agrees with the experimental result that the AFM-1 and AFM-2 regions are distinct and likely are not continuously connected through the NO x region, even at high P.

TABLE I. Hybridization energies between the αth $5f$ and the αth $3p$ orbitals in units of Rydbergs.

Δ_α	Si	P
$\Delta_{x(x^2-3y^2)}$	2.9796×10^{-2}	2.4191×10^{-2}
$\Delta_{y(y^2-3x^2)}$	2.9796×10^{-2}	2.4191×10^{-2}
Δ_{xyz}	1.3276×10^{-2}	1.0410×10^{-2}
$\Delta_{z(x^2-y^2)}$	1.5901×10^{-2}	1.3029×10^{-2}
$\Delta_{x(5z^2-r^2)}$	2.6998×10^{-2}	2.2109×10^{-2}
$\Delta_{y(5z^2-r^2)}$	2.6998×10^{-2}	2.2109×10^{-2}
$\Delta_{z(5z^2-3r^2)}$	2.1279×10^{-3}	1.5357×10^{-3}

These results further clarify the factors that control the complex electronic and magnetic behavior that is seen in URu_2Si_2 and shed some light on how it relates to its chemical analogs. In particular, it appears that the dual quantities of hybridization strength and charge tuning act as entangled axes to set the ground-state behavior. Applied pressure and Ru $\rightarrow$ Fe/Os substitution tune primarily along the hybridization axis, while nonisoelectronic tuning at the Ru or Si site is a combination of hybridization and charge tuning. Despite the complexity of this situation, we note that electron dopings (Ru $\rightarrow$ Co, Rh [32–37], Ir [33], or Si $\rightarrow$ P [47,48]) all produce similar phase diagrams that eventually feature ordering that is phenomenologically similar to AFM-2, while hole dopings (Ru $\rightarrow$ Mn [39], Tc [33,39], Re [33,38–43]) suppress the HO/AFM boundary but produce ferromagnetism at large doping. This universality raises the possibility that the several compounds closely related to URu_2Si_2 that have magnetic ground states (e.g., UCo_2Si_2 [55], URh_2Si_2 [53], UIr_2Si_2 [53,54], UNi_2Ge_2 [68], and UCr_2Si_2 [69]) might eventually be driven into the hidden order state using tailored chemical substitution. In order to do this, it will be necessary to reexamine and expand the knowledge about the Fermi surfaces and electronic hybridization characteristics of these other U-based compounds that form in the same crystalline structure.

V. CONCLUSIONS

Temperature-dependent electrical resistivity measurements were performed under applied pressures P up to 20 kbar in the chemical substitution series $URu_2Si_{2-x}P_x$. Specimens in the HO x region show similarities to the parent compound, where HO transforms into antiferromagnetism (AFM-1) at a critical pressure (P_c). P_c decreases with increasing x and collapses towards $P = 0$ near $x \approx 0.03$, suggesting that AFM-1 occurs at ambient pressure for this concentration. No pressure-induced phase transitions are observed in the NO x region and the AFM-2 state is only weakly suppressed by P. Measurements further reveal that AFM-1 and AFM-2 are distinct from each other. In order to better understand these phenomena, tight-binding Hartree-Fock calculations were performed, which show (i) that the radial probability distributions for the phosphorus ions are more tightly bound than that of the silicon and (ii) that the energy difference between the orbitals decreases with increasing x. The cumulative effect of these two factors is that Si $\rightarrow$ P substitution decreases the hybridization strength, which correlates with the weakening of HO. At larger x, additional effects such as electrical charge tuning also play an important role in determining the ground-state behavior. Additional measurements, such as angle-resolved photoelectron spectroscopy, that directly measure the Fermi surface will be needed to establish this possibility.

ACKNOWLEDGMENTS

We would like to thank Jun Lu for the use of his equipment. This work was performed at the National High Magnetic Field Laboratory, which is supported by National Science Foundation Cooperative Agreement No. DMR-1644779 and the State of Florida. Synthesis of crystalline materials and their characterization were supported by the Center for Actinide Science and Technology (CAST), an Energy Frontier Research Center (EFRC) funded by the U.S. Department of Energy (DOE), Office of Science, Basic Energy Sciences (BES), under Award No. DE-SC0016568.

[1] T. T. M. Palstra, A. A. Menovsky, J. van den Berg, A. J. Dirkmaat, P. H. Kes, G. J. Nieuwenhuys, and J. A. Mydosh, Phys. Rev. Lett. **55**, 2727 (1985).
[2] M. B. Maple, J. W. Chen, Y. Dalichaouch, T. Kohara, C. Rossel, M. S. Torikachvili, M. W. McElfresh, and J. D. Thompson, Phys. Rev. Lett. **56**, 185 (1986).
[3] W. Schlabitz, J. Baumann, B. Pollit, U. Rauchschwalbe, H. M. Mayer, U. Ahlheim, and C. D. Bredl, Z. Phys. B **62**, 171 (1986).
[4] T. T. M. Palstra, A. A. Menovsky, and J. A. Mydosh, Phys. Rev. B **33**, 6527 (1986).
[5] C. Broholm, J. K. Kjems, W. J. L. Buyers, P. Matthews, T. T. M. Palstra, A. A. Menovsky, and J. A. Mydosh, Phys. Rev. Lett. **58**, 1467 (1987).
[6] K. Matsuda, Y. Kohori, T. Kohara, K. Kuwahara, and H. Amitsuka, Phys. Rev. Lett. **87**, 087203 (2001).
[7] A. F. Santander-Syro, M. Klein, F. L. Boariu, A. Nuber, P. Lejay, and F. Reinert, Nat. Phys. **5**, 637 (2009).
[8] R. Yoshida, Y. Nakamura, M. Fukui, Y. Haga, E. Yamamoto, Y. Ōnuki, M. Okawa, S. Shin, M. Hirai, Y. Muraoka, and T. Yokoya, Phys. Rev. B **82**, 205108 (2010).
[9] J.-Q. Meng, P. M. Oppeneer, J. A. Mydosh, P. S. Riseborough, K. Gofryk, J. J. Joyce, E. D. Bauer, Y. Li, and T. Durakiewicz, Phys. Rev. Lett. **111**, 127002 (2013).
[10] C. Bareille, F. L. Boariu, H. Schwab, P. Lejay, F. Reinert, and A. F. Santander-Syro, Nat. Commun. **5**, 4326 (2014).
[11] D. A. Bonn, J. D. Garrett, and T. Timusk, Phys. Rev. Lett. **61**, 1305 (1988).
[12] A. R. Schmidt, M. H. Hamidian, P. Wahl, F. Meier, A. V. Balatsky, J. D. Garrett, T. J. Williams, G. M. Luke, and J. C. Davis, Nature **465**, 570 (2010).
[13] P. Aynajian, E. H. da Silva Neto, C. V. Parker, Y. Huang, A. Pasupathy, J. Mydosh, and A. Yazdani, Proc. Natl. Acad. Sci. USA **107**, 10383 (2010).
[14] J. S. Hall, U. Nagel, T. Uleksin, T. Rõõm, T. Williams, G. Luke, and T. Timusk, Phys. Rev. B **86**, 035132 (2012).
[15] R. P. S. M. Lobo, J. Buhot, M. A. Méasson, D. Aoki, G. Lapertot, P. Lejay, and C. C. Homes, Phys. Rev. B **92**, 045129 (2015).
[16] H.-H. Kung, R. E. Baumbach, E. D. Bauer, V. K. Thorsmølle, W.-L. Zhang, K. Haule, J. A. Mydosh, and G. Blumberg, Science **347**, 1339 (2015).
[17] J. A. Mydosh and P. M. Oppeneer, Rev. Mod. Phys. **83**, 1301 (2011).
[18] J. A. Mydosh, P. M. Oppeneer, and P. S. Riseborough, J. Phys.: Condens. Matter **32**, 143002 (2020).

[19] F. D. Boer, J. Franse, E. Louis, A. Menovsky, J. Mydosh, T. Palstra, U. Rauchschwalbe, W. Schlabitz, F. Steglich, and A. D. Visser, Phys. B+C **138**, 1 (1986).

[20] G. J. Nieuwenhuys, Phys. Rev. B **35**, 5260 (1987).

[21] K. H. Kim, N. Harrison, M. Jaime, G. S. Boebinger, and J. A. Mydosh, Phys. Rev. Lett. **91**, 256401 (2003).

[22] K. H. Kim, N. Harrison, M. Jaime, G. S. Boebinger, and J. A. Mydosh, Phys. Rev. Lett. **91**, 269902(E) (2003).

[23] M. W. McElfresh, J. D. Thompson, J. O. Willis, M. B. Maple, T. Kohara, and M. S. Torikachvili, Phys. Rev. B **35**, 43 (1987).

[24] G. Motoyama, T. Nishioka, and N. K. Sato, Phys. Rev. Lett. **90**, 166402 (2003).

[25] E. Hassinger, G. Knebel, K. Izawa, P. Lejay, B. Salce, and J. Flouquet, Phys. Rev. B **77**, 115117 (2008).

[26] N. P. Butch, J. R. Jeffries, S. Chi, J. B. Leão, J. W. Lynn, and M. B. Maple, Phys. Rev. B **82**, 060408(R) (2010).

[27] N. Kanchanavatee, M. Janoschek, R. E. Baumbach, J. J. Hamlin, D. A. Zocco, K. Huang, and M. B. Maple, Phys. Rev. B **84**, 245122 (2011).

[28] N. Kanchanavatee, B. White, V. Burnett, and M. Maple, Philos. Mag. **94**, 3681 (2014).

[29] P. Das, N. Kanchanavatee, J. S. Helton, K. Huang, R. E. Baumbach, E. D. Bauer, B. D. White, V. W. Burnett, M. B. Maple, J. W. Lynn, and M. Janoschek, Phys. Rev. B **91**, 085122 (2015).

[30] M. N. Wilson, T. J. Williams, Y.-P. Cai, A. M. Hallas, T. Medina, T. J. Munsie, S. C. Cheung, B. A. Frandsen, L. Liu, Y. J. Uemura, and G. M. Luke, Phys. Rev. B **93**, 064402 (2016).

[31] S. Ran, C. T. Wolowiec, I. Jeon, N. Pouse, N. Kanchanavatee, B. D. White, K. Huang, D. Martien, T. DaPron, D. Snow, M. Williamsen, S. Spagna, P. S. Riseborough, and M. B. Maple, Proc. Natl. Acad. Sci. USA **113**, 13348 (2016).

[32] H. Amitsuka, K. Hyomi, T. Nishioka, Y. Miyako, and T. Suzuki, J. Magn. Magn. Mater. **76-77**, 168 (1988).

[33] Y. Dalichaouch, M. B. Maple, J. W. Chen, T. Kohara, C. Rossel, M. S. Torikachvili, and A. L. Giorgi, Phys. Rev. B **41**, 1829 (1990).

[34] Y. Miyako, S. Kawarazaki, H. Amitsuka, C. C. Paulsen, and K. Hasselbach, J. Appl. Phys. **70**, 5791 (1991).

[35] S. Kawarazaki, Y. Kobashi, T. Taniguchi, Y. Miyako, and H. Amitsuka, J. Phys. Soc. Jpn. **63**, 716 (1994).

[36] M. Yokoyama, H. Amitsuka, S. Itoh, I. Kawasaki, K. Tenya, and H. Yoshizawa, J. Phys. Soc. Jpn. **73**, 545 (2004).

[37] M. Yokoyama and H. Amitsuka, J. Phys. Soc. Jpn. **76**, 136 (2007).

[38] Y. Dalichaouch, M. B. Maple, M. S. Torikachvili, and A. L. Giorgi, Phys. Rev. B **39**, 2423 (1989).

[39] Y. Dalichaouch, M. B. Maple, R. P. Guertin, M. V. Kuric, M. S. Torikachvili, and A. L. Giorgi, Phys. B **163**, 113 (1990).

[40] E. D. Bauer, V. S. Zapf, P.-C. Ho, N. P. Butch, E. J. Freeman, C. Sirvent, and M. B. Maple, Phys. Rev. Lett. **94**, 046401 (2005).

[41] J. R. Jeffries, N. P. Butch, B. T. Yukich, and M. B. Maple, Phys. Rev. Lett. **99**, 217207 (2007).

[42] N. P. Butch and M. B. Maple, Phys. Rev. Lett. **103**, 076404 (2009).

[43] N. P. Butch and M. B. Maple, J. Phys.: Condens. Matter **22**, 164204 (2010).

[44] A. L. de la Torre, P. Visani, Y. Dalichaouch, B. Lee, and M. Maple, Phys. B **179**, 208 (1992).

[45] J.-G. Park, S. B. Roy, and B. R. Coles, J. Phys.: Condens. Matter **6**, 5937 (1994).

[46] J.-G. Park and B. Coles, Phys. B **206-207**, 418 (1995).

[47] A. Gallagher, K.-W. Chen, C. M. Moir, S. K. Cary, F. Kametani, N. Kikugawa, D. Graf, T. E. Albrecht-Schmitt, S. C. Riggs, A. Shekhter, and R. E. Baumbach, Nat. Commun. **7**, 10712 (2016).

[48] A. Gallagher, K.-W. Chen, S. K. Cary, F. Kametani, D. Graf, T. E. Albrecht-Schmitt, A. Shekhter, and R. E. Baumbach, J. Phys.: Condens. Matter **29**, 024004 (2016).

[49] K. Murata, K. Yokogawa, H. Yoshino, S. Klotz, P. Munsch, A. Irizawa, M. Nishiyama, K. Iizuka, T. Nanba, T. Okada, Y. Shiraga, and S. Aoyama, Rev. Sci. Instrum. **79**, 085101 (2008).

[50] G. J. Piermarini, S. Bloch, J. D. Barnett, and R. A. Forman, J. Appl. Phys. **46**, 2774 (1975).

[51] J. R. Jeffries, N. P. Butch, B. T. Yukich, and M. B. Maple, J. Phys.: Condens. Matter **20**, 095225 (2008).

[52] G. Motoyama, N. Yokoyama, A. Sumiyama, and Y. Oda, J. Phys. Soc. Jpn. **77**, 123710 (2008).

[53] A. M. Umarji, J. V. Yakhmi, C. V. Tomy, R. M. Iyer, L. C. Gupta, and R. Vijayaraghavan, in *Theoretical and Experimental Aspects of Valence Fluctuations and Heavy Fermions*, edited by L. C. Gupta and S. K. Malik (Springer, Boston, MA, 1987), pp. 341–344.

[54] A. Vernière, S. Raymond, J. X. Boucherle, P. Lejay, B. Fåk, J. Flouquet, and J. M. Mignot, J. Magn. Magn. Mater. **153**, 55 (1996).

[55] M. Mihalik, A. Kolomiets, J.-C. Griveau, A. V. Andreev, and V. Sechovský, High Press. Res. **26**, 479 (2006).

[56] C. T. Wolowiec, N. Kanchanavatee, K. Huang, S. Ran, and M. B. Maple, Phys. Rev. B **94**, 085145 (2016).

[57] See Supplemental Material at http://link.aps.org/supplemental/10.1103/PhysRevB.102.245152 for details on the atomic Hartree-Fock calculations, including wave functions, binding energies, and $3p$-$5f$ hybridization energies, which includes Refs. [58–67].

[58] J. C. Slater, Phys. Rev. **35**, 210 (1930).

[59] V. Fock, Z. Phys. **61**, 126 (1930).

[60] J. C. Slater, Phys. Rev. **81**, 385 (1951).

[61] G. J. Rozing, P. E. Mijnarends, and D. D. Koelling, Phys. Rev. B **43**, 9515 (1991).

[62] T. Koopmans, Physica **1**, 104 (1934).

[63] M. Wolfsberg and L. Helmholz, J. Chem. Phys. **20**, 837 (1952).

[64] J. C. Slater and G. F. Koster, Phys. Rev. **94**, 1498 (1954).

[65] J. A. Gaunt and R. H. Fowler, Philos. Trans. R. Soc. A **228**, 151 (1929).

[66] K. Lendi, Phys. Rev. B **9**, 2433 (1974).

[67] K. Takegahara, Y. Aoki, and A. Yanase, J. Phys. C **13**, 583 (1980).

[68] Y. B. Ning, J. D. Garrett, C. V. Stager, and W. R. Datars, Phys. Rev. B **46**, 8201 (1992).

[69] T. D. Matsuda, N. Metoki, Y. Haga, S. Ikeda, K. Kaneko, E. Yamamoto, and Y. Onuki, J. Phys.: Condens. Matter **15**, S2023 (2003).